

Modelling of heat, mass and charge transfer in a PEMFC single cell

J. Ramousse, J. Deseure, O. Lottin, S. Didierjean*, D. Maillet

Laboratoire d'Énergétique et de Mécanique Théorique et Appliquée, UMR 7563 CNRS, INPL, UHP, 2, Avenue de la Forêt de Haye, BP 160, 54504 Vandoeuvre, France

Accepted 7 January 2005
Available online 1 June 2005

Abstract

The aim of this study is the understanding of the main phenomena governing fuel cell performances. We present a fuel cell model that takes into account gas diffusion in the porous electrodes, water diffusion and electro-osmotic transport through the polymeric membrane, and heat transfer in both the Membrane Electrodes Assembly (MEA) and bipolar plates. This model is constructed by combining independent descriptions of heat and mass transfers in the cell with a third description of coupled charge and mass transfers in the electrodes, considered porous.

The results show that thermal gradients in the MEA could lead to thermal stresses at high current densities. The feeding gas temperature influence on the cell temperature is also important.

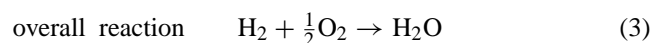
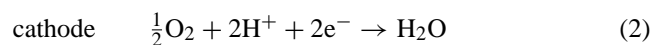
© 2005 Elsevier B.V. All rights reserved.

Keywords: PEMFC; Modelling; Gas diffusion electrode; Heat transfer; Mass transfer; Fuel cell

1. Introduction

Compared to thermodynamic machines used for electricity production, one of the main advantages associated with fuel cells is that they are not limited by Carnot efficiency. Besides, no moving part is required to convert chemical energy into electric energy. In this paper, we consider Proton Exchange Membrane Fuel Cells (PEMFCs): PEMFCs are composed of a polymer electrolyte sandwiched between two porous backing layers to form a Membrane Electrode Assembly (MEA). The electrodes (the active layers) are inserted between the electrolyte and the backing layers. Following Springer et al. [1], we refer to the backing and active layers (considered together but without the membrane) as the Gas Diffusion Electrodes (GDE). The MEA is located between two graphite bipolar plates, which collect electric current and allow gas feeding and system cooling. At the anode, H_2 is oxidized (1), liberating electrons and producing protons. The electrons flow to the cathode via an external

circuit, where they combine with the protons and the oxidant (oxygen) to produce water (2). Proton transfer from the anode to the cathode through the polymer membrane closes the electrical circuit. The overall reaction (3) differs from hydrogen combustion because part of the Gibbs free energy can be converted into electric energy



A careful water management is necessary to ensure that the membrane remains fully hydrated, in order to improve the ionic conductivity and to avoid electrodes flooding. This occurs when an excess of liquid water restrains the species access to the active layers. Water saturation pressure being a strong and non-linear function of temperature, water management is closely linked to thermal management. Both water and thermal managements are key issues for PEMFCs systems.

Various models help to understand the MEA behaviour. According to Bernardi and Verbrugge [2] and Jaouen et al.

* Corresponding author. Tel.: +33 3 83 59 55 60.

E-mail address: sophie.didierjean@ensem.inpl-nancy.fr (S. Didierjean).

Nomenclature

b_i	tafel slope ($V \text{ dec}^{-1}$)
$c_{\text{H}_2\text{O}}$	water concentration (mol m^3)
d_{pore}	pore diameter (m)
D_{ij}	diffusion coefficients of species i to j ($\text{m}^2 \text{ s}^{-1}$)
D_m	effective diffusion coefficients of water in the membrane ($\text{m}^2 \text{ s}^{-1}$)
D_{ij}^{eff}	effective diffusion coefficients ($\text{m}^2 \text{ s}^{-1}$)
D_{ij}^{K}	Knudsen diffusion coefficient ($\text{m}^2 \text{ s}^{-1}$)
EW	equivalent weight (kg mol^{-1})
E_{cell}	cell potential (V)
E^0	standard potential (V)
F	Faraday's constant (C mol^{-1})
h	convective heat transfer coefficient ($\text{W m}^{-2} \text{ K}^{-1}$)
$\text{HR}_{\text{a,c}}$	relative humidities (–)
i_f	Faradic current density (A m^{-2})
$i_{0(i)}$	exchange current density (A m^{-2})
J_{cell}	total current density (A m^{-2})
L	thickness (m)
$L_V^{\text{H}_2\text{O}}$	latent heat of water evaporation (kJ mol^{-1})
M_i	molar weight (kg mol^{-1})
N	density of molar flux ($\text{mol m}^{-2} \text{ s}$)
Nu	Nombre de Nusselt (–)
P	pressure (Pa)
P_i	partial pressure (Pa)
P_{sat}	saturated vapor pressure (Pa)
\dot{Q}	surfacic heat sources (W m^{-2})
Q_J	volumetric heat source in the membrane (W m^{-3})
R	Universal gas constant ($\text{J mol}^{-1} \text{ K}^{-1}$)
y_i	molar rate of the gas species i (–)
Z	thermal resistance (W m^{-2})

Greek letters

γ	roughness factor (–)
δ	size of the agglomerate (m)
ε	porosity (–)
$\varepsilon_{\text{a,c}}^{\text{eff}}$	effective porosity (in the agglomerate) (–)
η_i	overpotential (V)
κ	thermal conductivities ($\text{W m}^{-1} \text{ K}^{-1}$)
λ	water content in the membrane (–)
ξ	tortuosity (–)
ρ_{dry}	dry Nafion [®] density (kg m^{-3})
σ_{H^+}	protonic conductivity (S m^{-1})
$\sigma_{\text{H}^+}^{\text{eff}}$	effective protonic conductivity (S m^{-1})
τ_o	osmotic coefficient (mol mol^{-1})
ϕ	thermal flux (W m^{-2})

Subscripts

a	anode
act	active layers

b	backing layers
BP	bipolar plates
c	cathode
H_2	hydrogen
H_2O	water
m	membrane
N_2	nitrogen
O_2	oxygen

[3], since water is produced at the cathode, the impact of water management on cathode performances is significant at high current densities. However, these authors do not model mass transfer in the whole MEA. Experimental works of Buchi and Srinivasan [4] confirmed the importance of gas hydration and Sena et al. [5] emphasized the links between water transport in the membrane, membrane thickness and feeding gases composition. According to these authors, the ionic transport through the membrane is the limiting phenomenon when the gas hydration is low. On the other hand, they also showed that the access of gases to catalytic surfaces becomes a limiting factor when the membrane is sufficiently hydrated [5]. Costamagna [6,7] and Okada et al. [8], who modelled the charge and mass transfers inside the MEA in steady state or in transient conditions, confirmed these observations.

The literature proposes various ways to predict the electrochemical behaviour of electrodes. Springer et al. [1,9] proposed analytical formulations and emphasized the capacitive and resistive effects of oxygen reduction. Song et al. [10] and Eikerling and Kornyshev [11] completed these information by their descriptions of the electrode microstructure. This must be considered in order to explain the electrodes electrochemical behaviour and to estimate the overvoltage. Thus, Rowe and Li [12] took into account the volumetric characteristics of the active layer while considering it as a homogeneous and non-porous mixture of polymer, carbon and catalyst [13].

The model of Rowe and Li [12] also predicts the temperature gradients inside the MEA as well as their consequences on PEMFC performances. Similarly, Fuller and Newman [14] showed that temperature distributions depend on mass balance. They emphasized the need to control well the membrane hydration and PEMFC operating temperature. Yan et al. [15] show that the temperature could affect water distribution inside the membrane. This can be damaged at high current density.

Although most of the models used are one-dimensional, they correctly predict the electrochemical behaviour of MEA. However, Costamagna [6,7] and Djilali and Lu [16] suggested that a multidimensional model could improve the description, since gas composition and temperature vary along the feeding channels.

The model presented in this work describes, in steady state, one-dimensional heat and mass transfers in the whole cell and charge and mass transfers in the electrodes. It is constructed by combining independent descriptions of heat and mass transfers in the cell with a third description of coupled charge and mass transfers in the electrodes. Results of the whole cell mass transfer model are used as boundary conditions in the electrode model, which provides information about heat sources, necessary to determine heat fluxes in the MEA. The heat transfer model also requires data about water fluxes or gas velocity coming from the cell mass transfer model. Finally, this description of heat, mass and charge transfers allows the prediction of the thermal, concentration and potential fields in a single cell.

2. Theoretical models

2.1. Geometric description

A PEMFC single cell can be described schematically (Fig. 1) as an assembly of seven layers constituting four distinct areas:

- On both sides of the MEA, the bipolar plates cumulate three functions: thermal control thanks to cooling water channels, gas feeding via the gas channels and current collector.
- The porous backing layers made of carbon fibres coated with hydrophobic PTFE ensure a homogeneous gas distribution on the electrodes and limit liquid water accumulation in the MEA.
- The active layers are thin layers of platinum dispersed on carbon particles embedded in the polymer electrolyte. The catalyzed electrochemical and chemical reactions occur in these layers.
- Only protons and water can go through the polymer membrane located at the centre of the assembly.

Considering the low thickness of the active layers, more than 100 times thinner than the others components of the

MEA, the electronic and ionic transfers occurring in these areas are assumed to be without significant consequence on the mass transfer in the whole cell. Charge and mass transfers in the electrodes are considered in order to evaluate their electrochemical behaviour. The overvoltages are then interpreted in term of heat sources in the heat transfer model. Let us note that mass and charge transfers are always calculated assuming that the MEA is isothermal. The operating conditions are always chosen in order to avoid water condensation in the backing layers and the gas mixtures are assumed to obey the ideal gas law.

2.2. Mass transfer in the whole MEA

The source terms are the molar flux densities of hydrogen and oxygen consumed (negative sign) at the anode and at the cathode, respectively, and the molar flux density of water produced at the cathode (positive sign). They are given by the following expressions:

$$N_{\text{H}_2} = -\frac{J_{\text{cell}}}{2F}, \quad N_{\text{O}_2} = -\frac{J_{\text{cell}}}{4F}, \quad N_{\text{H}_2\text{O}} = \frac{J_{\text{cell}}}{2F} \quad (4)$$

The membrane being impervious to gases, hydrogen and oxygen only flows from the bipolar plates to the anode and to the cathode, respectively. Only water can go through the membrane, in a direction depending on current density and on gas hydration (5) [8]. Fluxes are considered positive in the x -direction (Fig. 1)

$$N_{\text{H}_2\text{O}}^c = \frac{J_{\text{cell}}}{2F} + N_{\text{H}_2\text{O}}^m \quad \text{and} \quad N_{\text{H}_2\text{O}}^a = N_{\text{H}_2\text{O}}^m \quad (5)$$

Most of the models encountered in the literature use Stefan–Maxwell equations to describe the diffusion of gas in the backing layers (6) [1]:

$$\frac{dy_i}{dx} = \frac{RT}{P} \sum_j \frac{y_i N_j - y_j N_i}{D_{ij}^{\text{eff}}} \quad (6)$$

and

$$\sum_i y_i = 1 \text{ at both anode and cathode sides} \quad (7)$$

with $i, j = \text{H}_2, \text{H}_2\text{O}_{\text{gas}}$ at the anode side and $i, j = \text{O}_2, \text{N}_2, \text{H}_2\text{O}_{\text{gas}}$ at the cathode side.

The backing layers being porous, it is necessary to use effective diffusion coefficients (8) [17]:

$$D_{i,j}^{\text{eff}} = \varepsilon_b^{2/3} D_{i,j} \quad (8)$$

The anode and cathode thickness are neglected: the electrodes are considered as interfaces between the membrane and the backing layers.

Considering the molar flux densities of water in the backing layer (4) as parameters, and using the concentrations of gases in the bipolar plates feeding channels as boundary conditions, Eq. (6) lead to the following analytic expressions for the species concentration distributions (9)–(14).

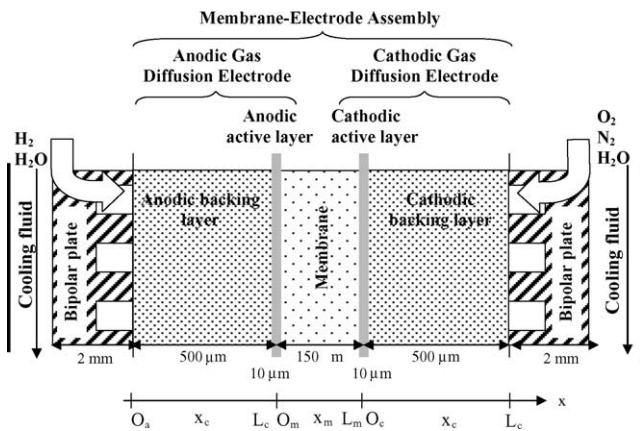


Fig. 1. Schematic description of the PEMFC single cell.

In the anodic backing layer:

if $N_{H_2} + N_{H_2O_a} \neq 0$

$$y_{H_2}(x_a) = \frac{N_{H_2}}{N_{H_2} + N_{H_2O_a}} + y_{H_2}^0 - \frac{N_{H_2}}{N_{H_2} + N_{H_2O_a}} \exp(k_a x_a) \quad (9)$$

with

$$k_a = \frac{[N_{H_2}] + N_{H_2O_a}}{cD_{H_2, H_2O}^{eff}},$$

$$c = \frac{P}{RT}, \quad y_{H_2O_a}(x_a) = 1 - y_{H_2}(x_a)$$

if $N_{H_2} + N_{H_2O_a} = 0$

$$y_{H_2}(z_a) = -\frac{N_{H_2}}{cD_{H_2, H_2O}^{eff}} x_a + y_{H_2}^0 \quad (10)$$

with $y_{H_2O_a}(x_a) = 1 - y_{H_2}(x_a)$.

In the cathodic backing layer:

if $k_n - k_c \neq 0$

$$y_{N_2}(x_c) = y_{N_2}^0 \frac{\exp(k_n x_c)}{\exp(k_n l)} \quad (11)$$

with

$$k_n = \frac{N_{H_2O_c}}{cD_{N_2, H_2O}^{eff}} + \frac{N_{O_2}}{cD_{N_2, O_2}^{eff}}$$

$$y_{O_2}(x_c) = \left(y_{O_2}^0 - \frac{N_{O_2}}{cD_{O_2, H_2O}^{eff}} \frac{1}{k_c} - \frac{y_{N_2}^0 N_{O_2}}{k_n - k_c} \left(\frac{1}{cD_{O_2, H_2O}^{eff}} - \frac{1}{cD_{O_2, N_2}^{eff}} \right) \right) \frac{\exp(k_c x_c)}{\exp(k_c l)} + \frac{y_{N_2}^0 N_{O_2}}{k_n - k_c} \left(\frac{1}{cD_{O_2, H_2O}^{eff}} - \frac{1}{cD_{O_2, N_2}^{eff}} \right) \frac{\exp(k_n x_c)}{\exp(k_n l)} + \frac{N_{O_2}}{cD_{O_2, H_2O}^{eff}} \frac{1}{k_c} \quad (12)$$

with

$$k_c = \frac{N_{H_2O_c} + N_{O_2}}{cD_{O_2, H_2O}^{eff}}$$

and

$$y_{H_2O}(x_c) = 1 - y_{O_2}(x_c) - y_{N_2}(x_c)$$

if $k_n - k_c = 0$

$$y_{N_2}(x_c) = y_{N_2}^0 \frac{\exp(k_n x_c)}{\exp(k_n l)} \quad (13)$$

$$y_{O_2}(x_c) = \left(y_{O_2}^0 - \frac{N_{O_2}}{cD_{O_2, H_2O}^{eff}} \frac{1}{k_c} \right) \frac{\exp(k_c x_c)}{\exp(k_c l)} + y_{N_2}^0 N_{O_2} \left(\frac{1}{cD_{O_2, H_2O}^{eff}} - \frac{1}{cD_{O_2, N_2}^{eff}} \right) \times \left(\frac{x_c \exp(k_c x_c) - l \exp(k_c l)}{\exp(k_n l)} \right) + \frac{N_{O_2}}{cD_{O_2, H_2O}^{eff}} \frac{1}{k_c} \quad (14)$$

where $y_{H_2}^0$, $y_{O_2}^0$ and $y_{N_2}^0$ are molar concentrations in the gas channels.

Bernardi and Verbruge [2] describe water transport in the polymer membrane using Darcy equations completed by a supplementary term representing the electro-osmotic water transfer due to electric field and proton flux. We do not retain this description, which needs a high number of parameters, some of them difficult to evaluate. The phenomenological model of water transport in the membrane proposed by Springer et al. [1] is used here. In this model, the water content (λ) of the membrane is defined as the number of water moles per mole of sulfonic acid

$$\lambda = \frac{EW}{\rho_{dry}} c_{H_2O} \quad (15)$$

where EW (equivalent weight) represents the dry membrane weight per mole of sulfonate group (kg mol^{-1}); ρ_{dry} is the density of dry polymer (kg m^{-3}).

According to Okada et al. [8], the water electro-osmotic flux through the membrane, always directed from anode to cathode, is a linear function of the proton flux imposed by the current density:

$$N_{H_2O}^{osmotic} = \tau \frac{J_{cell}}{F} \quad \text{and} \quad \tau = \lambda \tau_o \quad (16)$$

where τ stands for the water molecules number dragged by a proton [8]. τ_o is the electro-osmotic drag coefficient (Table 1).

Table 1
Parameters used in mass transfer model

Parameter	Value	Refs.
$L_a = L_c$	$230 \times 10^{-6} \text{ m}$	This work
L_m	$125 \times 10^{-6} \text{ m}$	This work
ε_{back}	0.8	[1]
EW	1.1 kg mol^{-1}	[8]
ρ_{dry}	2020 kg m^{-3}	[8]
τ_o	2.5/22	[8]
D_m	$3 \times 10^{-10} \text{ m}^2 \text{ s}^{-1}$	[8]
D_{H_2/H_2O}^{eff}	$1.63 \times 10^{-4} \text{ m}^2 \text{ s}^{-1}$	[20]
D_{O_2/H_2O}^{eff}	$3.20 \times 10^{-5} \text{ m}^2 \text{ s}^{-1}$	[20]
D_{O_2/N_2}^{eff}	$2.41 \times 10^{-5} \text{ m}^2 \text{ s}^{-1}$	[20]
D_{H_2O/N_2}^{eff}	$3.35 \times 10^{-5} \text{ m}^2 \text{ s}^{-1}$	[20]

The water diffusion flux $N_{\text{H}_2\text{O}}^{\text{diff}}$ through the membrane depends linearly on the water concentration gradient. The sum of diffusion and electro-osmotic fluxes yields a first order differential equation in the λ variable:

$$N_{\text{H}_2\text{O}}^{\text{m}} = N_{\text{H}_2\text{O}}^{\text{osmotic}} + N_{\text{H}_2\text{O}}^{\text{diff}} = \lambda \tau_0 \frac{J_{\text{cell}}}{F} - D_{\text{m}} \frac{\rho_{\text{dry}}}{\text{EW}} \frac{d\lambda}{dx} \quad (17)$$

And the solution of Eq. (17) is:

$$N_{\text{H}_2\text{O}}^{\text{m}} = \frac{\tau_0 J_{\text{cell}}}{F} \left[\lambda_{\text{a}} + \frac{\lambda_{\text{c}} - \lambda_{\text{a}}}{1 - \exp(k_{\text{m}} L_{\text{m}})} \right] \quad (18)$$

with

$$k_{\text{m}} = \frac{\text{EW} \tau_0 J_{\text{cell}}}{\rho_{\text{dry}} D_{\text{m}} F}$$

λ_{c} and λ_{a} stand for polymer water content at the membrane/cathode and membrane/anode interfaces, respectively. Then, assuming thermodynamic equilibrium between water vapor in the backing layers and liquid water in the polymer, the sorption curve of Hinatsu et al. [18] is used to associate partial pressure values to λ_{a} and λ_{c} :

$$\lambda = 0.3 + 10.8 \left(\frac{p_{\text{H}_2\text{O}}}{P_{\text{sat}}} \right) - 16 \left(\frac{p_{\text{H}_2\text{O}}}{P_{\text{sat}}} \right)^2 + 14.1 \left(\frac{p_{\text{H}_2\text{O}}}{P_{\text{sat}}} \right)^3 \quad (19)$$

The solving algorithm determines the water concentrations at the GDE/membrane interfaces that satisfy Eq. (5). The membrane ionic conductivity depends on its temperature and water content, according to the correlation of Neubrand [19]:

$$\sigma_{\text{H}^+} = e^{(-E_{\text{A}}(1/t-1/353))} (0.0013\lambda^3 + 0.0298\lambda^2 + 0.2658\lambda) \quad (20)$$

with

$$E_{\text{A}} = 2640 e^{(-0.6\lambda)} + 1183 \quad (21)$$

And the ohmic drop is given by:

$$\eta_{\text{m}} = J_{\text{cell}} \int_0^{L_{\text{m}}} \frac{1}{\sigma_{\text{H}^+}(x)} dx \quad (22)$$

The values of the main parameters used in this model are summarized in Table 1.

2.3. Active layers equations

Considering the results of a cylindrical model of pores inside the electrode, Srinivasan and Hurwitz [21] assert that it is preferable to use a volumetric description of the active layer and a formalism of the Butler–Volmer type than to use a description derived from Tafel law. The agglomerate model [22] that assumes the presence of macro-pores in the electrodes, seems to be well adapted to the PEMFC anode and cathode. Siegel et al. [23] used it to simulate the electrochemical behaviour of a MEA. Thanks to this kind of model, it is

possible to investigate in details the physicochemical mechanisms taking place in the electrodes:

- Gas concentration variation in the pores.
- Agglomerate protonic conductivity dependence on hydration.
- Microstructural effects (platinum loading, agglomerate size).

However, there are phenomena disparities linked to water transfers in the fuel cell, since under high current densities the anode will tend to be dehydrated and cathode to be flooded. Under these conditions the model assumptions are not identical for both electrodes.

Fig. 2 represents schematically the simplified pore structure assumed in the agglomerate model. The solid phase consists of a homogeneous mixture of polymer electrolyte (Nafion®), carbon, and catalyst (Pt).

The active layer thickness L_{act} , the agglomerate (assumed cylindrical) diameter δ and the porosity ε_{act} characterize the active layer geometry. The active layer porosity ε_{act} is defined by:

$$\varepsilon_{\text{act}} = \frac{V_{\text{pore}}}{V_{\text{pore}} + V_{\text{agg}}} = \frac{S_{\text{pore}}}{S_{\text{pore}} + S_{\text{agg}}} \quad (23)$$

where S_{agg} is the agglomerate section and S_{pore} is the pore section.

And the pore equivalent diameter can be estimated by:

$$d_{\text{pore}} = \frac{\varepsilon_{\text{act}}}{1 - \varepsilon_{\text{act}}} \delta \quad (24)$$

As mentioned by Middelmann [24], the best electrodes performances are achieved with the highest possible ratio L_{act}/δ . The electrodes electrochemical behaviour also

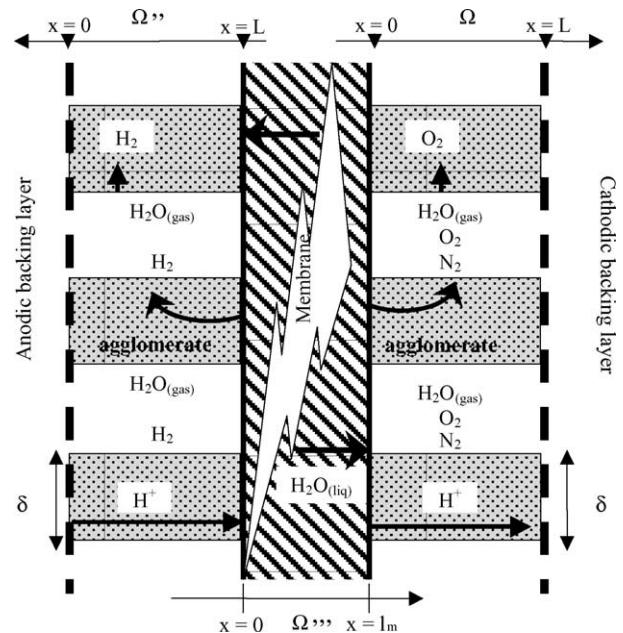


Fig. 2. Schematic description of the active layers.

depends on a last parameter, the specific area, which is a function of the catalyst load W_{Pt} (g m^{-2}) and is recurrently expressed as follows:

$$\gamma = \frac{\text{active platinum area}}{\text{MEA section}} \quad (25)$$

In the agglomerate, both an ionic current density and an electronic current density flow. They vary with the x coordinate. The ionic current density is nil at the active layer/backing layer interfaces ($x=0$) and the electronic density is nil at the membrane/active layers interfaces ($x=L_{act}$). In steady state, the local variation of the electronic current density is the opposite of the local variation of the ionic current density; it is also equal to the faradaic current density i_f . The cell current density J_{cell} is the sum (over the electrode thickness L_{act}) of the faradaic current density:

$$J_{cell} = \frac{\gamma}{L_{act}} \int_0^L i_f dx \quad (26)$$

2.3.1. Anode model

PEMFCs anode is seldom studied. Boyer et al. [25] assert that the ionic conductivity of the active layer influences the electrochemical performances of the electrodes. Furthermore, due to electro-osmotic water flux in the membrane, the polymer of the anode agglomerate is more prone to dehydration than that of the cathode [26]. Considering this, it seems appropriate that the anode model takes into account both the ohmic drop in the active layer and the hydrogen concentration variations in the gas pores. This modelling of the ionic transfer completes the description of Rowe and Li [12] for mass transfer in the non-porous active layer.

The main assumptions of the anode model are the following:

1. Mass transfer of H_2O and H_2 is considered only in the gas pores, there is no diffusion of water in the agglomerate.
2. The H_2O concentration in the agglomerate is imposed by thermodynamic equilibrium with the gas phase.
3. The ionic conductivity of the agglomerate is a function of the ionic conductivity of the polymer, which depends on its water content.
4. Only the migration of protons is considered in the agglomerate.
5. Pressure and temperature are uniform.

The Stefan–Maxwell equations [1] completed by a supplementary term for Knudsen diffusion in the small pores of the active layer [17] describe diffusion of hydrogen and water in the gas phase:

$$\frac{dy_i}{dx} = \frac{RT}{P} \left(\sum_j \left[\frac{y_i N_j - y_j N_i}{D_{ij}} \right] - \frac{N_i}{D_i^k} \right) \quad (27)$$

the Knudsen diffusion coefficient D_i^k being expressed as follows [17]:

$$D_i^k = d_{pore} \frac{\xi}{3\varepsilon_{act}} \sqrt{\frac{8RT}{\pi M_i}} \quad (28)$$

with d_{pore} and ε_{act} given by Eqs. (23) and (24).

The hydrogen consumption in the gas pores of the active layer yields the following mass balance equation:

$$\frac{\partial N_{\text{H}_2}^a}{\partial x} + \frac{\gamma}{L_{act}} \frac{i_f}{2F} = 0 \quad (29)$$

And the water mass balance leads to:

$$\frac{\partial N_{\text{H}_2\text{O}}^a}{\partial x} = 0 \quad (30)$$

The boundary conditions of Eqs. (27), (29) and (30) are given by the output of the mass transfer model in the whole cell:

- Concentration of each species at the active layer/backing layer interfaces (9)–(10).
- Molar flux density of water and hydrogen (4)–(5).

The overpotential distribution Eq. (33) in the active layer can be calculated by means of the proton balance (31) and Ohm's law (32) in the ionic phase:

$$\frac{\partial i}{\partial x} = \frac{\gamma}{L_{act}} i_f \quad (31)$$

$$\frac{\partial \eta_a}{\partial x} = \frac{i}{\sigma_{\text{H}^+}^{\text{eff}}} \quad (32)$$

$$\frac{d(\sigma_{\text{H}^+}^{\text{eff}} d\eta)}{dx^2} - \frac{\gamma}{L_{act}} i_f = 0 \quad (33)$$

The effective ionic conductivity of the agglomerate depends on Nafion®'s conductivity [19] (20) and (21), which is simply corrected as a function of the agglomerate polymer content, $\varepsilon_{\text{Nafion}}$:

$$\sigma_{\text{H}^+}^{\text{eff}}(x) = \varepsilon_{\text{Nafion}} \sigma_{\text{H}^+}(x) \quad (34)$$

Since the polymer water content λ depends, via the sorption curves (19), on water partial pressure in the gas pores, the agglomerate ionic conductivity is thus a function of the x co-ordinate; differential equation (31) has to be solved with the following boundary conditions:

- The ionic current density is nil at the active layer/backing layer interface $\left(-\sigma_{\text{H}^+}^{\text{eff}} \frac{d\eta}{dx} \Big|_0 = 0 \right)$.
- Electrode overpotential at the membrane/active layer interface is known ($\eta(x = L_{act}) = \eta_0$). In practice, η_0 is adjusted until J_{cell} equals the value used for the determination of hydrogen consumption (4).

The solution of Eqs. (31)–(33) yields the distributions of concentrations and electrodes overpotential as function of x -coordinate.

Two mechanisms are commonly associated with hydrogen oxidation on platinum in acid mixture: Heyrovsky–Volmer and Tafel–Volmer [27]. With a fast Volmer step, which is usually the case in strong acid media, the oxidation kinetics can be written as follows:

$$i_f = i_{0(\text{H}_2)} \left(e^{(2.3/b_{\text{H}_2})\eta_a(x)} \frac{y_{\text{H}_2}}{y_{\text{H}_2}^*} - e^{-(2.3/b^*)\eta_a(x)} \right) \quad (35)$$

where $y_{\text{H}_2}^*$ is the hydrogen concentration at the open-circuit.

2.3.2. Cathode model

According to the majority of the authors, fuel cells lack of efficiency (in terms of electrochemical conversion) is due mostly to phenomena occurring at the cathode. Kim et al. [28] compared the results of their models to experimental data in various operating conditions and concluded that the oxygen reduction process is limiting. The cathode being the place of water production, it is reasonable to assume that ionic resistivity of the well-hydrated polymer can be neglected. However, oxygen access to the catalyst sites remains problematic, not only because of the flooding risk, but also due to its low partial pressure. As Bernardi and Verbruge [2] proposed, a one-dimensional model can describe the cathode operation by taking into account only oxygen diffusion in the gas pores and reduction kinetics.

The main assumptions of the cathode model are the following:

1. Mass transfer of H_2O and O_2 is considered only in the gas pores.
2. Diffusion of water in the agglomerate is neglected.
3. The ohmic drop in the active layer is neglected.
4. Pressure and temperature are uniform.

Gas diffusion inside the cathodic gas pores is described by Stefan–Maxwell equations modified to take account of Knudsen diffusion ((27) and (28)). Oxygen consumption and water production in the porous active layer yield the following mass balance equations:

$$\frac{\partial N_{\text{N}_2}^c}{\partial x} = 0 \quad (36)$$

$$\frac{\partial N_{\text{O}_2}^c}{\partial x} + \frac{\gamma}{L_{\text{act}}} \frac{i_f}{4F} = 0 \quad (37)$$

$$\frac{\partial N_{\text{H}_2\text{O}}^c}{\partial x} - \frac{\gamma}{L_{\text{act}}} \frac{i_f}{2F} = 0 \quad (38)$$

Once again, the boundary conditions of Eqs. (27), (36)–(38) are given by results of the mass transfer model in the whole cell:

- Concentration of each species at the backing layer/active layer interfaces (11)–(14).
- Molar flux density of water and oxygen (4)–(5).

Table 2

Parameter used in the active layer models

Parameter	Value	Refs.
L	10×10^{-6} m	This work
δ	3×10^{-6} m	[23]
ε_{act}	$0.3 \text{ m}^3 \text{ m}^{-3}$	This work
$\varepsilon_{\text{Nafion}}$	$0.5 \text{ m}^3 \text{ m}^{-3}$	This work
ξ	1.7	This work
γ	$100 \text{ m}^2 \text{ m}^{-2}$	[27]
$b_{\text{H}_2} = b_{\text{H}_2}^*$	30 mV dec^{-1}	[27]
$i_{0(\text{H}_2)}$	$1 \times 10^{-2} \text{ A cm}^{-2}$	[27]
$b_{\text{O}_2} = b_{\text{O}_2}^*$	120 mV dec^{-1}	[27]
$i_{0(\text{O}_2)}$	$4 \times 10^{-7} \text{ A cm}^{-2}$	[27]

A Butler–Volmer law [3,22,29] is generally used to describe oxygen reduction kinetics in acid media (Nafion[®]):

$$i_f = i_{0(\text{O}_2)} \left(e^{(2.3/b_{\text{O}_2})|\eta_{\text{c}}|} \frac{y_{\text{O}_2}}{y_{\text{O}_2}^*} - e^{-(2.3/b_{\text{O}_2}^*)|\eta_{\text{c}}|} \right) \quad (39)$$

2.3.3. Main parameters and overvoltage calculation

The cell potential is determined by means of the following expressions:

$$E_{\text{cell}} = E^0 - \eta_a|_{x=0} + \eta_c - \eta_m \quad (40)$$

$$E^0 = -\frac{\Delta G(T, P)}{2F} \quad (41)$$

where $\Delta G(T, P)$ is given by the Nernst equation and η_m is a result of the cell mass transfer model (22). η_a ($x=0$) (35) and η_c (39) are estimated thanks to the GDE models with parameters whose values are reported in Table 2.

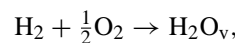
2.4. Heat transfer in the single cell

Various phenomena are responsible for heat production by fuel cells [30]. Firstly, the ionic resistivity of the membrane through which protons flow is at the origin of a volumetric heat source distributed in its whole thickness (22):

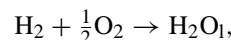
$$Q_j = J_{\text{cell}} \eta_m \quad (42)$$

Secondly, electrochemical reactions, and water sorption or desorption, imply heat production (or even consumption in some particular cases) at the electrodes. The heat production mechanisms occurring at the electrodes are the following:

- *Global reaction entropy*. Even in fully reversible conditions, the simultaneous hydrogen oxidation at the anode and oxygen reduction at the cathode produce heat (43)



$$T\Delta S = -4.7 \text{ kJ mol}^{-1} \text{ at } T = 298 \text{ K}$$



$$T\Delta S = -48.7 \text{ kJ mol}^{-1} \text{ at } T = 298 \text{ K} \quad (43)$$

$$\dot{Q}_a^{\text{reac}} + \dot{Q}_c^{\text{reac}} = \frac{-J_{\text{cell}} T \Delta S}{2F}$$

It is not easy to determine which part of the global reaction entropy must be attributed to each electrode: a quick review of the literature shows that, according to the authors, the half-reaction of hydrogen oxidation (1) can be isothermal ($\dot{Q}_a^{\text{reac}} = 0$) [31], endothermic ($\dot{Q}_a^{\text{reac}} < 0$) [32] or exothermic ($\dot{Q}_a^{\text{reac}} > 0$) [33]. In this paper the hydrogen oxidation is assumed isothermal and, consequently, the entropy of oxygen reduction (2) equals that of water formation reaction (43).

- *Electrode overpotentials* result from the electrodes models ((35) and (39)). The associated heat production is given by Eq. (44). The thickness of the electrodes is neglected in the heat transfer model

$$\dot{Q}_a^{\text{overpot}} = \eta_a(x=0) J_{\text{cell}}$$

$$\dot{Q}_c^{\text{overpot}} = |\eta_c| J_{\text{cell}} \quad (44)$$

- *Water sorption or desorption* at the GDE/membrane interfaces

$$\dot{Q}_a^{\text{sorp}} = \Delta H_S^{\text{H}_2\text{O}} N_{\text{H}_2\text{O}}^m \quad \text{and}$$

$$\dot{Q}_c^{\text{sorp}} = -\Delta H_S^{\text{H}_2\text{O}} N_{\text{H}_2\text{O}}^m \quad \text{with } \Delta H_S^{\text{H}_2\text{O}} > 0 \quad (45)$$

- Water being liquid in the polymer membrane and gaseous in the backing layers, the sorption and desorption phenomena are responsible for heat production or absorption, respectively. The enthalpy of sorption $\Delta H_S^{\text{H}_2\text{O}}$ is assumed equal to the latent heat of water vaporization $\Delta L_V^{\text{H}_2\text{O}}$ [34].

In steady state, heat transfer through the MEA is modelled using the energy equation applied to incompressible fluids with constant physical properties in porous media [35]. The volumetric heat source Q_J is nil in the backing layers

$$\kappa \frac{\partial^2 T}{\partial x^2} = \sum_i \varepsilon_i N_i \frac{\partial H_i}{\partial x} + (Q_J) \quad (46)$$

where ε_i is the i species volumetric fraction in the backing layer, defined such as $\sum_i \varepsilon_i^{b,m} = \varepsilon_{b,m}$. κ is the equivalent thermal conductivity of the porous media (Table 3). The molar

Table 3
Parameter used in heat transfer model

Parameter	Value	Refs.
L_{BP}	1×10^{-3} m	This work
ε_b	0.8	This work
ε_m	0.28	This work
κ_a, κ_c	$1.6 \text{ W m}^{-1} \text{ K}^{-1}$	[12,42]
κ_m	$0.34 \text{ W m}^{-1} \text{ K}^{-1}$	[12]
κ_{BP}	$100 \text{ W m}^{-1} \text{ K}^{-1}$	This work
$\Delta L_V^{\text{H}_2\text{O}}$	44 kJ mol^{-1}	[34]
h_{eau}	$2672 \text{ W m}^{-2} \text{ K}^{-1}$	This work
h_{H_2}	$824 \text{ W m}^{-2} \text{ K}^{-1}$	This work
h_{air}	$1200 \text{ W m}^{-2} \text{ K}^{-1}$	This work

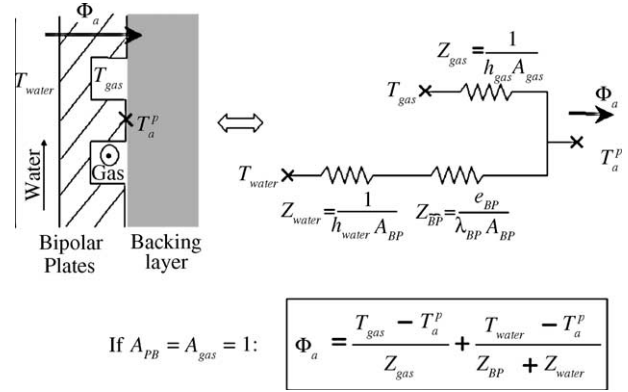


Fig. 3. Schematic description of heat transfer in the bipolar plates (example at the anode side).

flux densities of the species come from the cell mass transfer model (Section 2.2).

Enthalpy transport by protons and electrons is neglected. Temperature continuity and energy conservation at the GDE/membrane interfaces lead to the following equations:

$$-\kappa_a \frac{\partial T_a}{\partial x_a} \Big|_{x_a=L_a} + \dot{Q}_a = -\kappa_m \frac{\partial T_m}{\partial x_m} \Big|_{x_m=0} \quad (47)$$

$$-\kappa_m \frac{\partial T_m}{\partial x_m} \Big|_{x_m=L_m} + \dot{Q}_c = -\kappa_c \frac{\partial T_c}{\partial x_c} \Big|_{x_c=0} \quad (48)$$

with

$$\dot{Q}_{a,c} = \dot{Q}_{a,c}^{\text{overpot}} + \dot{Q}_{a,c}^{\text{reac}} + \dot{Q}_{a,c}^{\text{sorp}} \quad (49)$$

And the energy conservation at the GDE/bipolar plates interfaces gives:

$$\phi_a = -\kappa_a \frac{\partial T_a}{\partial x_a} \Big|_{x_a=0} \quad (50)$$

$$\phi_c = -\kappa_c \frac{\partial T_c}{\partial x_c} \Big|_{x_c=L_c} \quad (51)$$

$\phi_{a,c}$ is the heat flux density flowing through the bipolar plate, which depends on the feeding gas and cooling water temperatures. This heat flux density is evaluated thanks to a resistive model shown in Fig. 3. The heat transfer coefficients in the laminar water and gas flows are evaluated with correlation (52):

$$Nu_i = \frac{h_i d}{\lambda_i} = 4 \quad (52)$$

3. Results and discussion

3.1. Overpotentials

A literature review gives the three main types of models used to evaluate the overvoltages at both electrodes:

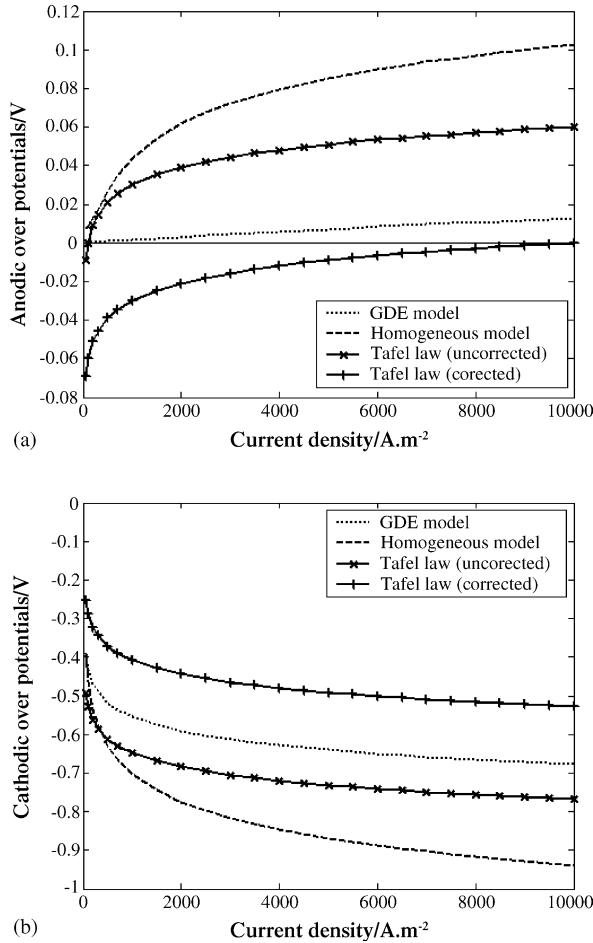


Fig. 4. (a) Influence of electrodes description on anodic overvoltages, (b) influence of electrodes description on cathodic overvoltages.

- The Tafel law results from experimental observations: this simple and widely used description is based on the following phenomenological equation:

$$\eta = b_i \log \left(\frac{J_{\text{cell}}}{i_{0(c,a)}} \right) \quad (53)$$

- The models of non-porous active layer (homogeneous model) proposed by Jaouen et al. [3] assume that the active layer is made up of an homogeneous mixture of catalyst and carbon powder embedded in electrolyte. The overpotential expression results from the use of Butler–Volmer equation:

$$J_{\text{cell}} = \gamma i_{0(a,c)} \left\{ \left[y_i^0 \exp \left(\frac{2.3\eta}{b_i} \right) - \exp \left(-\frac{2.3\eta}{b_i^*} \right) \right] \left(\frac{\tanh \left(\sqrt{\frac{\gamma i_{0(a,c)} L}{2FD_i^{\text{aggl}} y_i^0} \exp \left(\frac{2.3\eta}{b_i} \right)} \right)}{\sqrt{\frac{\gamma i_{0(a,c)} L}{2FD_i^{\text{aggl}} y_i^0} \exp \left(\frac{2.3\eta}{b_i} \right)}} \right) \right\} \quad (54)$$

where D_i^{aggl} is the coefficient of diffusion of the electroactive species in the homogeneous mixture.

- The GDE models [22,23] take into account the existence of gas pore (macro-pore) and (possibly) of the ohmic drop in the agglomerate.

Let us note that the same values of kinetic coefficients b_i and $i_{0(a,c)}$ can be used in these three models (Table 2). Fig. 4 depicts the evolutions of the cathodic and anodic overpotentials, calculated in the same operating conditions, as functions of the current density.

There are great differences between the overpotentials predicted by the three models, which emphasizes the important influence of the active layer on fuel cell performances. Particular attention should be paid to the use of Tafel law: the effective platinum area being higher than the MEA section, the exchange current density i_0 should be multiplied by a geometric parameter such as the roughness factor γ (55). In this case the anodic overvoltage becomes negative (Fig. 5). Actually, Tafel law is adapted only to high current density, far from thermodynamic equilibrium

$$\eta = b_i \log \left(\frac{J_{\text{cell}}}{\gamma i_{0(c,a)}} \right) \quad (55)$$

Some authors [36,37] propose to change the value of Tafel slope as a function of current density, which has the advantage to be a simple approach but does not provide information about the electrochemical processes. On the other hand, the porous and non-porous models require only intrinsic parameters: active layer thickness, platinum load (roughness factor) and Butler–Volmer kinetic coefficients. The polarization curves obtained with the porous and non-porous models exhibit Tafel behaviour. Due to the slow diffusion of active species in the homogeneous solid phase, the non-porous model tends to overestimate the overpotentials. GDE models do not have such drawbacks. Furthermore, they can simulate the electrode behaviour when the active layers porosity is low and when anode hydration is weak [25]. Only this model predicts an increasing potential drop in these two cases.

3.2. Thermal fields

The numerical results that are discussed in this section correspond to two different operating conditions:

- In Fig. 5a, both gases are humidified and preheated: $T_{\text{gas}}^a = T_{\text{gas}}^c = 80^\circ\text{C}$, $\text{HR}_a = 0.3$ and $\text{HR}_c = 0.6$.
- In Fig. 5b, only air is humidified and preheated ($T_{\text{gas}}^c = 70^\circ\text{C}$, and $\text{HR}_c = 0.9$) while hydrogen undergoes no treatment ($T_{\text{gas}}^a = 25^\circ\text{C}$, $\text{HR}_a = 0.1$).

Temperature fields are calculated for current densities ranging from 0 to 1 A cm⁻² in the first case (Fig. 5a), and from 0 to only 0.6 A cm⁻² in the second case (Fig. 5b); this last maximum value corresponding to a cell potential equal to zero. The temperature of the cooling circuit is set to 80 °C

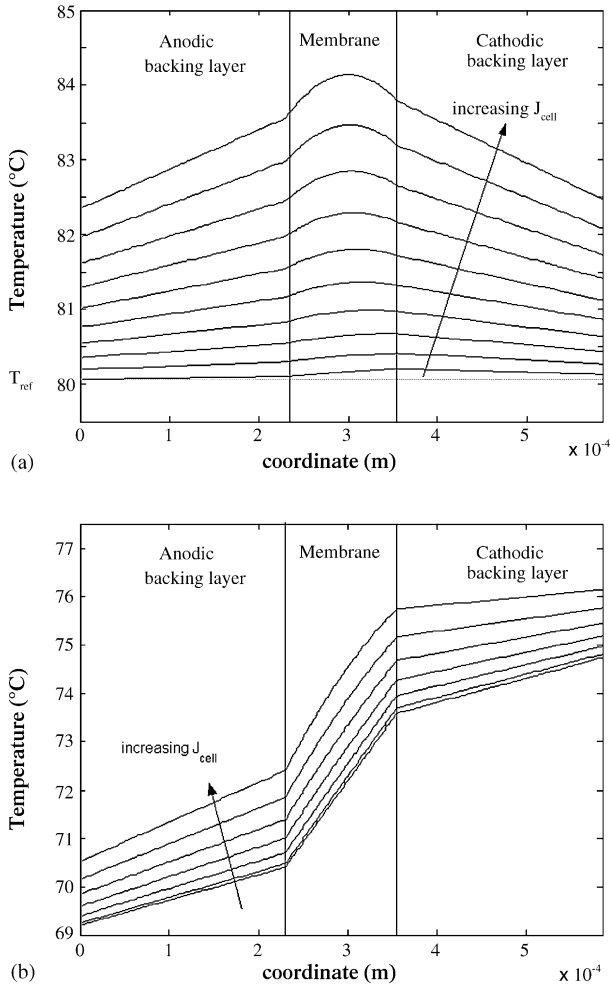


Fig. 5. (a) Temperature fields when both gases are preheated and humidified ($HR_a = 0.3$, $HR_c = 0.6$, $T_{water} = T_{gas}^a = T_{gas}^c = 80^\circ\text{C}$, J_{cell} from 0 to 1 A cm^{-2}). (b) Temperature fields for dry hydrogen ($HR_a = 0.1$, $HR_c = 0.9$, $T_{water} = 80^\circ\text{C}$, $T_{gas}^a = 25^\circ\text{C}$, $T_{gas}^c = 70^\circ\text{C}$, J_{cell} from 0 to 0.6 A cm^{-2}).

and the thermal properties of the MEA materials are those given in Table 3. The graphs give temperature distributions in the anodic backing layer ($0 \leq x \leq 230\ \mu\text{m}$), in the membrane ($230 \leq x \leq 355\ \mu\text{m}$) and in the cathodic backing layer ($355 \leq x \leq 585\ \mu\text{m}$). In the following, we define the fuel cell overheating as the maximum (positive) difference between the temperature of the MEA and that of the cooling water.

The linear temperature distributions in the backing layers are characteristic of purely conductive heat transfer. Indeed, the gas velocities being low ($v_{a,c}^{gas} \propto 10^{-3}\text{ m s}^{-1}$, $v_m^{H_2O} \propto 10^{-5}\text{ m s}^{-1}$), the convective contribution to heat transport can be neglected, as confirmed by the order of magnitude of Peclet number

$$Pe_m = \frac{\rho_{H_2O} v_m L_m}{\kappa_m} \leq 10^{-5} \quad (56)$$

$$Pe_{a,c} = \frac{\sum_i \rho_i v_i L_m}{\kappa_{a,c}} \leq 10^{-6} \quad (57)$$

Similarly, the temperature distribution in the membrane is representative of conductive heat transfer, but with a volumetric heat source.

The strong dependence of temperature fields on current density is linked to the physical mechanisms at the origin of the main heat sources: electrode overpotentials (44), Joule effect in the membrane (42) and reaction entropy (43). Nevertheless, heat generation or absorption due to water sorption or desorption by the membrane (45) is proportional to the water flux, which can be very important in the absence of electric current when there is a strong difference between water partial pressures in hydrogen and air.

The important difference between temperatures in the MEA and temperature of the cooling circuit must be emphasized. When both gases are humidified and preheated (Fig. 5a), the temperature in the membrane and in the active layers can be a few degrees above that of water. The thermal model presented in this study predicts MEA overheating of the same order of magnitude as those calculated by Djilali and Lu [16] but by taking into account the heat transfer resistances with water and gas, whose temperatures are used as parameters.

When the cell is fed with dry and cold hydrogen (Fig. 5b), the minimum temperature in the anodic backing layer can be 10°C below water temperature. This strong discrepancy is due to the cooling effect of cold hydrogen. The question, whether such temperature gradients could induce water condensation and thus anode flooding, will be tackled in a future work: it must be kept in mind that water saturation pressure is 50% higher at 80°C than at 70°C . Moreover, low hydrogen supply temperature generates thermal gradients in the membrane (close to 30°C mm^{-1}) that are more important than those due to Joule effect only (up to 10°C mm^{-1}).

Temperature gradients and MEA overheating are closely related to the backing layers thermal conductivity. The fibrous and porous nature of these layers does not allow a direct estimate of the equivalent thermal conductivity of the dry medium. The difference between values coming from various sources can reach one order of magnitude:

- Gurau et al. [39] and Wang et al. [38] used a equivalent conductivity of $19\text{ W m}^{-1}\text{ K}^{-1}$ determined with Maxwell model [40].
- Kjelstrup [41] proposed to use $\kappa_{a,c} = 0.2 \pm 0.1\text{ W m}^{-1}\text{ K}^{-1}$, value estimated from temperature measurements inside a single polymer fuel cell.
- And other authors [12] agree to assign a value of $1.6\text{ W m}^{-1}\text{ K}^{-1}$ to the backing layers equivalent thermal conductivity, as proposed by a manufacturer [42].

Repeated measurements performed on a specific bench, not presented here, gave us values of the order of $0.3\text{ W m}^{-1}\text{ K}^{-1}$ with *Quintech*TM carbon papers, which is close to Kjelstrup estimation. This value and those found in the literature are used to simulate temperature distributions in the MEA in the same operating conditions as those of Fig. 5a (both gas humidified and preheated and current

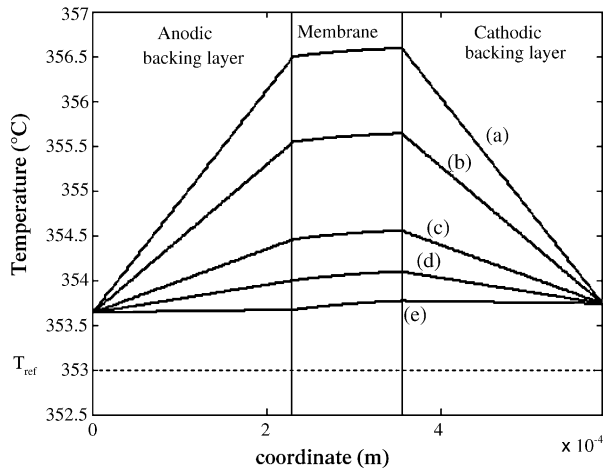


Fig. 6. Thermal distributions in the MEA for different values of thermal conductivities of the backing layers ($HR_a=0.3$, $HR_c=0.6$, $T_{\text{water}} = T_{\text{gas}}^a = T_{\text{gas}}^c = 80^\circ\text{C}$, (a) $\lambda = 0.2 \text{ W m}^{-1} \text{ K}^{-1}$; (b) $\lambda = 0.3 \text{ W m}^{-1} \text{ K}^{-1}$; (c) $\lambda = 0.7 \text{ W m}^{-1} \text{ K}^{-1}$; (d) $\lambda = 1.6 \text{ W m}^{-1} \text{ K}^{-1}$; (e) $\lambda = 19 \text{ W m}^{-1} \text{ K}^{-1}$).

density fixed to 0.5 A cm^{-2}). The results are presented in Fig. 6.

As shown in Fig. 6, the backing layers thermal conductivity has a great influence on temperature distributions. The MEA overheating increases with decreasing backing layers thermal conductivity, while the bipolar plates temperature stays quasi-constant due to the good graphite thermal conductivity. A first conclusion of these results is that the backing layers thermal conductivity is an important parameter to master, especially because of the (possible) presence of liquid water that can significantly modify its value. Another important conclusion is that temperature measurements performed directly on or inside the bipolar plates do not yield good estimates of the MEA temperature.

4. Conclusions and perspectives

A fuel cell model that takes into account gas diffusion in the porous electrodes, water diffusion and electro-osmotic transport through the polymeric membrane, and heat transfer in the Membrane Electrodes Assembly (MEA) and bipolar plates is presented. This model is constructed by combining independent descriptions of heat and mass transfers in the cell with a third description of coupled charge and mass transfers in the electrodes.

Based on a Butler–Volmer equation, the GDE description proposed in this paper requires only intrinsic parameters. It allows the evaluation of the anodic and cathodic overvoltages such as the simulated polarization curves exhibit a Tafel behaviour. Perspectives concerning the electrode behaviour could be the investigation of the effects of microstructure geometry and of the active layer ionic conductivity variations, particularly in the case of dry anode. Moreover, modifications of the active layer model will permit to simulate electrode flooding.

The results also show that thermal gradients in the MEA could lead to thermal stresses at high current densities. A discrepancy between the air and hydrogen feeding temperature increases these thermal stresses.

References

- [1] T.E. Springer, T.A. Zawodzinski, M.S. Wilson, S. Gottesfeld, *J. Electrochem. Soc.* 143 (2) (1996) 587–599.
- [2] D.M. Bernardi, M.W. Verbrugge, *AIChE J.* 37 (8) (1991) 1151–1163.
- [3] F. Jaouen, G. Lindbergh, G. Sundholm, *J. Electrochem. Soc.* 149 (4) (2002) A437–A447.
- [4] F.N. Buchi, S. Srinivasan, *J. Electrochem. Soc.* 144 (8) (1997) 2767–2772.
- [5] D.R. Sena, E.A. Ticianelli, V.A. Paganin, E.R. Gonzalez, *J. Electroanal. Chem.* 477 (1999) 164–170.
- [6] P. Costamagna, *Chem. Eng. Sci.* 56 (2001) 323–332.
- [7] P. Costamagna, *J. Power Sources* 102 (2001) 239–253.
- [8] T. Okada, G. Xie, Y. Tanabe, *J. Electroanal. Chem.* 413 (1996) 49–65.
- [9] T.E. Springer, I.D. Raistrick, *J. Electrochem. Soc.* 136 (6) (1989) 1594–1603.
- [10] H.K. Song, Y.H. Jung, K.H. Lee, L.H. Dao, *Electrochim. Acta* 44 (20) (1999) 3513–3519.
- [11] M. Eikerling, A.A. Kornyshev, *J. Electroanal. Chem.* 475 (1999) 107–123.
- [12] A. Rowe, X. Li, *J. Power Sources* 102 (2001) 82–96.
- [13] S. Srinivasan, H.D. Hurwitz, J.O'M. Bockris, *J. Chem. Phys.* 46 (8) (1967) 3108.
- [14] T.F. Fuller, J. Newman, *J. Electrochem. Soc.* 140 (1993) 1218–1225.
- [15] W.-M. Yan, F. Chen, H.-Y. Wu, C.-Y. Soong, H.-S. Chu, *J. Power Sources* 129 (2004) 127–137.
- [16] N. Djilali, D. Lu, *Inter. J. Therm. Sci.* 41 (2002) 29–40.
- [17] D. Armost, P. Schneider, *Chem. Eng. J.* 57 (1995) 91–99.
- [18] J.T. Hinatsu, M. Mizuhata, H. Takenaka, *J. Electrochem. Soc.* 141 (6) (1994) 1493–1498.
- [19] W. Neubrand, Thesis, Modelbildung und Simulation von Elektromembranverfahren, Logos, 1999.
- [20] R.B. Bird, W.E. Stewart, E.N. Lightfoot, *Transport Phenomena*, Wiley, New York, 1960.
- [21] S. Srinivasan, H.D. Hurwitz, *Electrochim. Acta* 12 (1967) 495–512.
- [22] F. Gloaguen, P. Convert, S. Gamburgzev, O.A. Velev, S. Srinivasan, *Electrochim. Acta* 43 (24) (1998) 3767–3772.
- [23] N.P. Siegel, M.W. Ellis, D.J. Nelson, M.R. von Spakovsky, *J. Power Sources* 115 (2003) 81–89.
- [24] E. Middelmann, *Fuel Cells Bull.* (2002) 9–12.
- [25] C. Boyer, S. Gamburgzev, O. Vlev, S. Srinivasan, A.J. Appleby, *Electrochim. Acta* 43 (24) (1998) 3703–3709.
- [26] D. Singh, D.M. Lu, N. Djilali, *Int. J. Eng. Sci.* 37 (1999) 431–452.
- [27] O. Antoine, Y. Bultel, R. Durand, P. Ozil, *Electrochim. Acta* 43 (1998) 3681–3691.
- [28] J. Kim, S.-M. Lee, S. Srinivasan, C.E. Chamberlin, *J. Electrochem. Soc.* 142 (8) (1995) 2670–2674.
- [29] Y. Bultel, L. Genies, O. Antoine, P. Ozil, R. Durand, *J. Electroanal. Chem.* 527 (2002) 143–155.
- [30] T.F. Fuller, J. Newman, *J. Electrochem. Soc.* 140 (5) (1993) 1218–1225.
- [31] M.J. Lampinen, M. Fomino, *J. Electrochem. Soc.* 140 (12) (1993) 3537–3546.
- [32] S. Kjelstrup, A. Rosjorde, ECOS 2003, Proceedings of the 16th International Conference on Efficiency, Costs, Optimization, Simulation and Environmental Impact of Energy Systems, Copenhagen, Denmark, June 30–July 2, 2003, pp. 921–928.
- [33] A.L. Rockwood, *Phys. Rev. A* 36 (3) (1987) 1525–1526.

- [34] P. Atkins, J. de Paula, *Physical Chemistry*, 7th ed., Oxford University Press, New York, 2002.
- [35] C. Moyne, S. Didierjean, H.P. Amaral Souto, O.T. da Silveira, *Int. J. Heat Mass Trans.* 43 (2000) 3853–3867.
- [36] A. Parthasarathy, S. Srinivasan, A.J. Appleby, C.R. Martin, *J. Electrochem. Soc.* 139 (9) (1992) 2530–2537.
- [37] F. Gloaguen, F. Andolfatto, R. Durand, P. Ozil, *J. Appl. Electrochem.* 24 (9) (1994) 863–869.
- [38] L. Wang, A. Husar, T. Zhou, H. Liu, *Int. J. Hydrogen Energ.* 28 (2003) 1263–1272.
- [39] V. Gurau, H. Liu, S. Kakaç, *AIChE J.* 44 (11) (1998) 2410–2422.
- [40] Corrélation de Maxwell pour les conductivités équivalentes de milieux poreux.
- [41] P.J.S. Vie, S. Kjelstrup, *Electrochim. Acta* 49 (2004) 1069–1077.
- [42] Toray Carbon Paper, Toray Industries, Inc., Advanced Composites Department, 2001.